Comprehensive analysis of Si-doped $Al_xGa_{1-x}As$ ($x=0$ to 1): Theory and experiments

Naresh Chand, Tim Henderson, John Klem, W. Ted Masselink, and Russ Fischer
Coordinated Science Laboratory, University of Illinois, 1101 West Springfield Avenue, Urbana, Illinois 61801

Yia-Chung Chang
Materials Research Laboratory, University of Illinois, 1101 West Springfield Avenue, Urbana, Illinois 61801

Hadis Morkoç
Coordinated Science Laboratory, University of Illinois, 1101 West Springfield Avenue, Urbana, Illinois 61801
(Received 16 April 1984)

Temperature-dependent Hall-effect measurements were carried out both in dark and in ambient light on Si-doped $Al_xGa_{1-x}As$ layers grown by molecular-beam epitaxy over the entire composition range. Above 150 K, the measured Hall carrier densities (different from actual electron densities near the direct-indirect transition) show an exponential dependence on temperature. A shallow donor (≤ 15 meV) tied to the Γ band and a deep donor level tied to the L band were observed. The deep donor is dominant for $x>0.2$, and its activation energy E_d rises dramatically up to the direct-indirect band-gap crossover and peaks at 160 meV for $x\sim 0.48$. As the Al fraction increases further, E_d decreases, reaching 57 meV for AlAs. The error due to multivalley conduction on the measured values of E_d is shown to be negligible. The variation in E_d of the dominant donor level with x is accounted for by our theoretical calculations using a multivalley effective-mass model. A decrease of E_d with increasing doping densities is also observed. At high substrate-growth temperature, the incorporation of Si atoms was found to decrease. The persistent-photoconductivity (PPC) effect was observed with an increase in mobilities over the dark values in the entire composition range. The effect was most pronounced in the range $0.20\leq x\leq 0.40$. Traps related to the Si-doping density appear to be responsible for the observed photoconductivity effect. The ratio of the PCC traps and the Si atomic density is maximum at $x\sim 0.32$ and is minimum in the direct-indirect band-gap crossover region.

I. INTRODUCTION

Recently, the $Al_xGa_{1-x}As$/GaAs material system grown by molecular-beam epitaxy (MBE) has received much attention because of its applications in a variety of high-performance heterojunction devices for switching, microwave, and optical applications. Invariably, these devices require the growth of n-type $Al_xGa_{1-x}As$ layers which can be accomplished by doping with, i.e., tellurium,[1–4] selenium,[3,5] tin,[3,6,7] and silicon.[8–15] Among these dopants, Si has been established as a nearly ideal n-type dopant for the growth of $Al_xGa_{1-x}As$/GaAs by MBE,[8,16] and has a sticking coefficient of nearly unity, small diffusivity, and allows good electrical and optical properties to be obtained.

The activation energy E_d of Te, Se, and Sn in $Al_xGa_{1-x}As$ was shown to be a few milli-electron-volts for compositions with $x\leq 0.22$, but for $x>0.22$ the activation energy was found to increase dramatically with increasing x up to the direct-indirect band-gap crossover point, and to decrease afterwards. The maximum value of E_d (Refs. 1–6 and 17) reported in the literature varied between 130 and 170 meV, assuming heavy compensation (i.e., using $n\propto\exp(-E_d/k_BT)$. However, Yang *et al.*[5] reported a maximum E_d of ~ 320 meV, but the relation they used was $n\propto\exp(-E_d/2k_BT)$, resulting in a difference of a factor of 2.

Despite many reports on the subject there is still a lack of sufficient experimental and theoretical details with regard to the activation energy, mobility, and persistent-photoconductivity (PPC) effect in Si-doped MBE-grown $Al_xGa_{1-x}As$ covering the entire composition range. Preliminary results on the properties of Si-doped $Al_xGa_{1-x}As$ (covering a few AlAs mole fractions), including the effect of the substrate and Si-cell temperatures on the Si-doping concentrations, were reported earlier.[11,12] The apparent activation energy in the heavily doped samples was found to be smaller than those reported for Se, Te, and Sn.[1–6] Künzel *et al.*[10] also made a similar observation and reported an activation energy of 13 meV for $x=0.35$ and $n=2\times 10^{17}$ cm^{-3} for Si donors. Ishikawa *et al.*[9] reported E_d for compositions $0\leq x\leq 0.5$ and found E_d to be maximized at $x=0.37$, whereas the behavior of Se (Ref. 5) and Sn (Ref. 6) suggests the maximum value of E_d to be at $x\sim 0.45$. Ishikawa *et al.* also found E_d to be independent of the donor concentration for samples with $x=0.27$ and 0.32. Morkoç *et al.*[7] and Künzel *et al.*,[10] however, found E_d to decrease with increasing electron concentration in Sn- and Si-doped samples, respectively. Most recently, Künzel *et al.*[18] reported a strong dependence of E_d on the doping concentration, with E_d varying from 22 to 125 meV for room-temperature doping densities ranging from 8.7×10^{17} to 7×10^{16} cm^{-3}, respectively. The present study demonstrates a behavior of donor ac-

tivation energy similar to that of the other dopants. The variation of E_d with x is explained using a multivalley effective-mass model.

As for the photosensitivity, several models have already been proposed to explain the PPC effect observed at low temperatures. When $Al_xGa_{1-x}As$ is exposed to light at temperatures below ~ 100 K, the apparent electron concentration as measured by the Hall effect increases. This increase persists for a long period of time even after the light is turned off. Nelson[2] and Lang *et al.*[4] observed a corresponding decrease in mobility, whereas Saxena,[19] Künzel *et al.*,[10] and we find an increase in mobility. Craford *et al.*[20] also noticed an increase in mobility in S-doped $GaAs_{1-x}P_x$ alloys. On the other hand, Collins *et al.*[14] observed a decrease in mobility in a sample with no $Al_xGa_{1-x}As$ buffer layer, but an increase in the other sample with a 1-μm-thick, undoped $Al_xGa_{1-x}As$ buffer layer. Since ionized-impurity scattering is dominant at low temperatures, the presence of donor-[2,4] and acceptor-type[19,20] traps were assumed to explain the decrease and increase of mobility, respectively. Collins *et al.*[14] suggested that the PPC was primarily due to photoinduced charge separation at the $Al_xGa_{1-x}As$/GaAs heterojunction. The decrease in mobility in the sample with no buffer layer was attributed to an increase in scattering resulting from ionized defect centers created by the photoexcitation of electrons. The increase in mobility in the sample with a 1-μm-thick buffer layer was attributed to the physical separation of electrons from their parent donors (two-dimensional electron gas).

The aim of this paper is to report our comprehensive theoretical and experimental study of Si-doped $Al_xGa_{1-x}As$ grown by MBE in the entire ($x=0$ to 1) composition range.

II. EXPERIMENTAL PROCEDURE

About 40 samples of $Al_xGa_{1-x}As$ with varying x were grown by MBE on {100}-oriented undoped semi-insulating GaAs substrates. The structures consisted of a 0.2-μm-thick, undoped GaAs buffer layer (to provide an atomically smooth surface on which to grow the AlGaAs), a 0.2-μm-thick buffer layer of undoped AlGaAs, graded in composition in some cases to prevent any modulation-doping effects, and a 1.0-μm-thick, Si-doped $Al_xGa_{1-x}As$ layer. For $x>0.50$, a (150–300)-Å-thick cap layer of undoped GaAs was also deposited to prevent oxidation of the AlAs-rich surface. Most layers reported here were grown at a substrate temperature of 610 °C as measured by an optical pyrometer. To investigate the influence of substrate temperature during growth, a few layers were also grown at 700 °C. A dimeric As source was used, resulting in high-quality layers even at substrate temperatures as low as 600 °C. For layers with $x>0.45$, the Al-effusion-cell temperature was kept constant at 1090 °C and the Ga-cell temperature was adjusted to obtain the desired mole fraction of AlAs. For other layers, both Ga- and Al-cell temperatures were systematically adjusted to keep the growth rate constant from layer to layer. The Si-cell temperature was varied between 975 and 1125 °C to control the Si flux. The substrates were mounted on a rotating holder to ensure compositional uniformity of the layers grown.

After the growth, the layers were characterized by Hall-effect measurements using the van der Pauw technique in a magnetic field of 3 kG and in the temperature range 10–300 K, both in dark as well as in ambient light. Cloverleaf patterns were defined photolithographically on (4×4)-mm^2-sized samples, and Ohmic contacts were formed by alloying tin dots at 400 °C in a H_2 atmosphere for ~ 2 min. The depletion effects caused by the pinning of the Fermi level by the surface and the band bending at the interface were neglected due to the relatively high doping levels used.[21]

The alloy composition of the direct-gap samples was determined by room-temperature photoluminescence (PL). For indirect-gap samples, x was estimated by measuring the thickness of the grown layer with a scanning electron microscope. The Al-cell temperature was held constant for $x>0.45$, and the growth rate of AlAs for that temperature was accurately calibrated by measuring the thickness of an AlAs layer. With this, the GaAs growth rate and thus the alloy composition could be extracted. In a few samples the compositions determined by the PL measurements were confirmed by a wavelength-dispersive x-ray analysis in a scanning electron microscope. Si atomic densities in the grown layers were estimated from *C-V* measurements of the donor concentrations in GaAs for various Si-cell temperatures.

III. RESULTS

A. Hall-effect measurements

The apparent (Hall) electron concentrations (n_H) obtained by using the simple relation $n_H=-1/eR_H$, are plotted in Fig. 1 against reciprocal temperatures for compositions $x=0.04$ to 1. To illustrate the influence of doping concentrations on the activation energies and the presence of shallow and deep donor levels, the Hall concentrations in widely used alloys of compositions of $x=0.29$ and 0.32 are plotted separately in Fig. 2. Room-temperature and 77-K data are also summarized in Table I for compositions $x>0.24$ which also illustrate the effect of PPC at 77 K. The PPC effect, which will be described later, is observed throughout the composition range, being very noticeable between $x=0.20$ and 0.40. To illustrate the PPC behavior, the electron concentration and mobility measured on sample 6 with $x=0.29$ both in dark and ambient light are plotted in Fig. 3. The carrier density with illumination was typically 1–5 % larger than the persistent density in the dark.

Figures 1–3 indicate that the freeze out of electrons is an exponential function of temperature between 300 and 150 K. For a nondegenerate semiconductor, the electron, donor, and acceptor concentrations (n, N_d, and N_a, respectively), and the activation energy (E_d), are related through the charge-neutrality condition,

$$\frac{n(N_a+n)}{N_d-N_a-n}=\frac{N_c}{g}\exp\left[\frac{-E_d}{k_B}T\right], \tag{1}$$

where g (=2) is the donor spin-degeneracy factor. Excit-

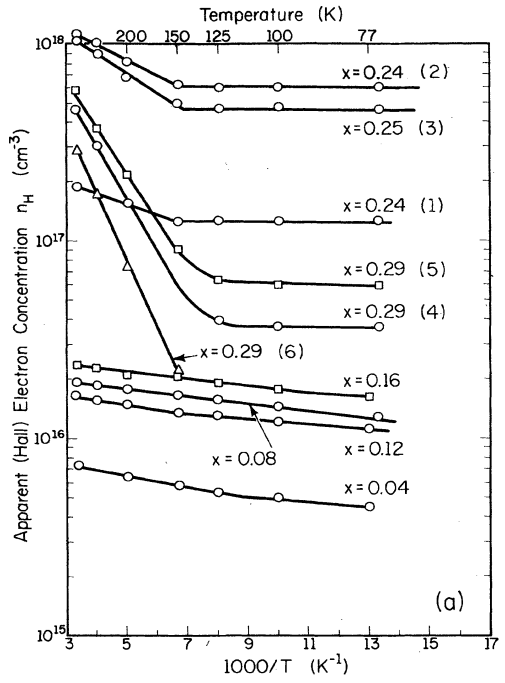

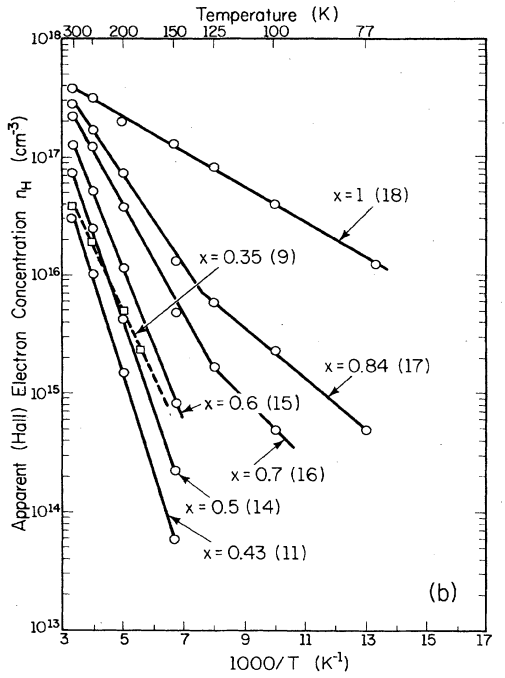

FIG. 1. Temperature dependence of the Hall electron concentration $(-1/eR_H)$ for Si-doped $Al_xGa_{1-x}As$ alloys: (a) for $x \leq 0.29$ and (b) for $x > 0.35$. The numbers in parentheses are the sample numbers referred to in Table I.

ed states of the donor atoms have been neglected in Eq. (1). To account for distribution of electrons in the Γ, L, and X conduction-band minima in $Al_xGa_{1-x}As$, the electron effective mass in the effective density of states, N_c, is given by[22]

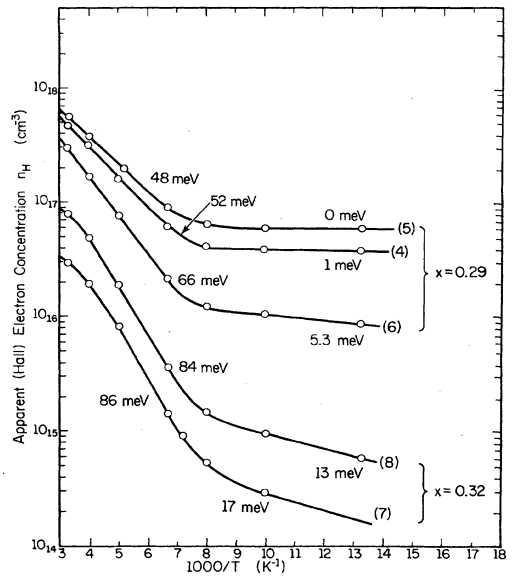

FIG. 2. Temperature dependence of the Hall electron concentration showing the influence of doping density on the activation energy. Also shown are the presence of deep and shallow donor levels. The alloy compositions are 0.29 and 0.32.

$$m^* = \left[\left[\frac{m_\Gamma^*}{m_0} \right]^{3/2} + \left[\frac{m_L^*}{m_0} \right]^{3/2} \exp\left[-\frac{\Delta E^{L-\Gamma}}{k_B T} \right] + \left[\frac{m_X^*}{m_0} \right]^{3/2} \exp\left[-\frac{\Delta E^{X-\Gamma}}{k_B T} \right] \right]^{2/3} \tag{2}$$

for $x < 0.45$, and, for $x > 0.45$,

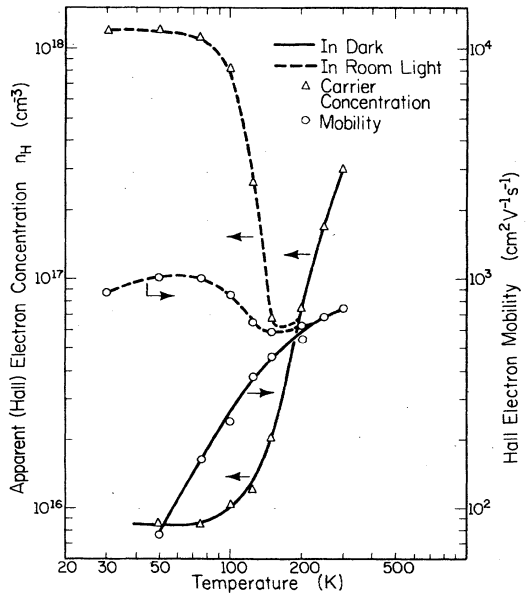

FIG. 3. Temperature dependence of Hall electron concentration and mobility for a Si-doped $Al_{0.29}Ga_{0.71-x}As$, sample 6. The solid and dashed curves represent the measured data in dark and room light, respectively.

TABLE I. Properties of Si-doped $Al_xGa_{1-x}As$ alloys grown by MBE.

Sample no.	x	Approximate values of N_{Si} (cm^{-3})	300 K n_H (cm^{-3})	300 K μ_H ($cm^{-2}V^{-1}s^{-1}$)	77 K Dark n_H (cm^{-3})	77 K Dark μ_H ($cm^{-2}V^{-1}s^{-1}$)	77 K Persistent n_H (cm^{-3})	77 K Persistent μ_H ($cm^2V^{-1}s^{-1}$)	E_d (meV)
1	0.24	2.5*E*17[c]	1.8*E*17	1940	1.2*E*17	1820	1.75*E*17	1930	22[a]
2	0.24	4.0*E*18	1.2*E*18	937	4.6*E*17	541	2.2*E*18	1170	17
3	0.25	4.0*E*18	1.1*E*18	880	6.0*E*17	691	2.1*E*18	1100	18
4	0.29	6.0*E*18	4.5*E*17	650	3.6*E*16	180	1.8*E*18	1000	52
5	0.29	6.0*E*18	5.7*E*17	696	5.8*E*16	294	2.0*E*18	1115	48
6	0.29	2.5*E*18	2.8*E*17	752	8.0*E*16	340	1.1*E*18	1000	66
7	0.32	4.5*E*16	2.9*E*16	1150			2.8*E*16	1212	86
8	0.32	2.5*E*17	7.8*E*16	1210	5.7*E*16	630	1.4*E*17	1190	84
9	0.35	2.5*E*17	3.8*E*15	1000			9.4*E*16	1110	108
10	0.36	2.5*E*17	9.0*E*15	1000			1.2*E*16	1690	130[b]
11	0.43	2.5*E*17	3.0*E*16	243			8.6*E*15	290	146
12	0.45	2.8*E*17	3.7*E*16	187			3.2*E*15	360	150
13	0.48	3.0*E*17	5.3*E*16	142			4.4*E*15	272	160
14	0.50	2.7*E*17	7.0*E*16	123			7.5*E*15	275	154
15	0.60	3.3*E*17	1.2*E*16	126					130
16	0.70	4.0*E*17	2.2*E*17	130	8.0*E*13	72	2.1*E*16	211	92
17	0.84	4.4*E*17	2.5*E*17	139	4.8*E*14	104	1.8*E*16	205	76
18	1.0	4.4*E*17	3.7*E*17	161	1.2*E*16	149	1.3*E*16	128	57[a]

[a] $n \propto \exp(-E_d/2k_BT)$ used; for all other samples, $n \propto \exp(-E_d/k_BT)$.
[b] Substrate temperature is 700 °C; for all other samples, 610 °C.
[c] *E*15 means $\times 10^{15}$, *E*16 means $\times 10^{16}$, *E*17 means $\times 10^{17}$, etc.

$$m^* = \left[\left[\frac{m_\Gamma^*}{m_0} \right]^{3/2} \exp\left[-\frac{\Delta E^{\Gamma-X}}{k_BT} \right] + \left[\frac{m_L^*}{m_0} \right]^{3/2} \exp\left[-\frac{\Delta E^{L-X}}{k_BT} \right] + \left[\frac{m_X^*}{m_0} \right]^{3/2} \right]^{2/3}, \tag{3}$$

where ΔE^{i-j} is the energy difference between i and j conduction-band minima, and m_i^* is the density-of-states electron effective mass in band i.

The straight lines in Figs. 1 and 2 show that the factor $(N_a+n)/(N_d-N_a-n)N_c$ in Eq. (1) either remains constant or varies exponentially with temperature. In order to determine an effective thermal activation energy of the dominant Si donor level, this term as a first approximation may be considered either constant or proportional to n depending upon whether $N_a \gg n$ (heavy compensation) or $N_a \ll n$ (negligible compensation), respectively. The term N_d is generally greater than N_a+n as the temperature is reduced, and any of the above two conditions should be true at low temperatures. In these two limiting cases the slope of the straight lines of the n-versus-T^{-1} curves in Figs. 1 and 2 should be either $-E_d/k_B$ or $-E_d/2k_B$, respectively.

To determine the nature of the slope of the n-versus-T^{-1} curves, values of N_d were calculated self-consistently using both values of E_d [given by $-E_d/k_B$ and $-E_d/2k_B$ in Eq. (1)] and compared with the estimated Si atomic density (N_{Si}). With the exception of sample 1, the slopes $-E_d/2k_B$ gave much higher values of N_d than expected from the fluxes used for $0.24 \leq x \leq 0.85$. However, the slope $-E_d/k_B$ gave values of N_d close to the expected ones. In the calculations, the measured electron concentrations n_H were corrected for the multivalley conduction which will be discussed later. Thus, the $Al_xGa_{1-x}As$ alloy in the range $0.24 \leq x \leq 0.85$ was considered highly compensated. Similar observations were also made recently by Saxena and Singh.[23] By determining which slope, $-E_d/k_B$ or $-E_d/2k_B$, is self-consistent with N_d, the values of E_d were calculated from the curves in Figs. 1 and 2. For $x<0.2$ this technique could not be used since the values of N_d obtained from both slopes were similar and the difference was within experimental error. In this range the samples were considered uncompensated and the slope in these cases was taken as $-E_d/2k_B$. The values of E_d so determined are summarized in Table I and plotted in Fig. 4. Owing to the surface and interface depletion effects,[21] if any, and due to the multivalley conduction, which will be discussed later, the actual carrier concentrations may be higher than shown in Figs. 1–3. As the temperature variation of these effects in the (300–150)-K range is negligible, the slopes of the n-versus-T^{-1} curves, and hence the activation energies will not change.

B. Effect of doping levels

Figure 2 illustrates the effect of the doping levels on the measured activation energies for compositions $x=0.29$ and 0.32, which are widely used in modulation-doped field-effect transistors (MODFET's). This figure also shows the presence of two donor levels for these alloy compositions. One is deep and dominates the conduction process in the (300–150)-K range; the other is shallow and dominant below 125 K. The initial freeze out is to the deep level, and once the deep levels are saturated the freeze out is to the shallow level. The impurity conduction will also contribute at low temperatures.

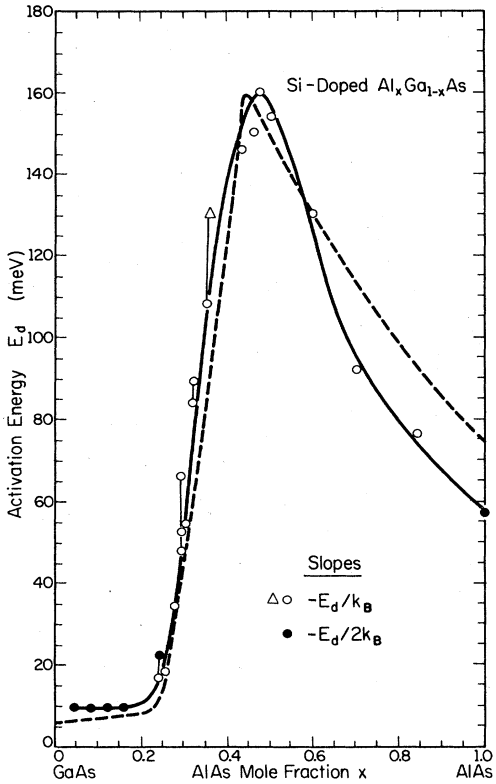

FIG. 4. Compositional dependence of the ionization energy E_d of the dominant Si donor level in $Al_xGa_{1-x}As$. The solid line connects experimental data points and the dashed line is obtained from theoretical calculations using a multivalley effective-mass model. The solid and open circles represent the slopes $-E_d/2k_B$ and $-E_d/k_B$, respectively. Only the layer (△) was grown at 700 °C; all others were grown at 610 °C substrate temperature. The vertical bars show variation of E_d with doping concentration at a given x. E_d decreases with increasing the doping level.

It is evident from Fig. 2 that the depth of both deep and shallow donors decreases with increasing doping densities. This is a well-known effect and occurs due to broadening of the donor level at high doping densities. The high-activation-energy points in Fig. 4 for a given alloy composition correspond to low doping concentrations, which lead to an increase in E_d. However, the effect of doping on E_d observed here is not as large as reported for composition $x=0.35$, most recently by Künzel *et al.*[18]

The room-temperature electron concentration in most cases is found to be lower than the Si atomic density. This is due to the fact that a large number of Si atoms remain unionized and some Si atoms are perhaps incorporated as acceptors due to the amphoteric nature of Si.

C. Composition dependence of the activation energy

The continuous line drawn through the experimental points in Fig. 4 represents the alloy-composition dependence of the activation energy of the Si donor level which dominates between 300 and 150 K for moderate doping levels. The spread in experimental points in Fig. 4, which is represented by vertical bars, at a given x, is due to the variation in the doping levels used and perhaps due to some uncertainty in the alloy compositions which were determined within 1% of accuracy.

E_d remains less than 10 meV for $x<0.2$ and starts rising at $x\sim0.2$ to a value of ~60 meV at $x=0.3$, reaching a maximum of 160 meV at $x\sim0.48$, where the band gap has changed from direct to indirect. For $x>0.48$, E_d decreases monotonically and reaches a value of ~57 meV for AlAs. This variation of the Si-donor energy level with x in $Al_xGa_{1-x}As$ is similar to the previously observed behavior of other donor impurities.[1–6,17] For $0.22<x<0.40$, E_d for moderate doping levels can be approximately expressed as

$$E_d \cong 707x - 146 \text{ meV} . \quad (4)$$

The values of E_d for $x>0.5$ differ somewhat among various reports. This may be attributed to (i) the lack of a detailed study as the alloy in this range is not very useful for semiconductor applications, (ii) the uncertainty in determining the AlAs mole fraction, and (iii) the nonuniformity of the AlAs composition in the liquid-phase-epitaxy— (LPE-) grown layers due to a high distribution coefficient of Al (earlier studies were made on LPE-grown materials). For $x<0.2$ the values of E_d reported earlier are ~5 meV,[6,9] whereas we have shown a value of ~9 meV. The difference is a result of the fact that in this alloy range we have taken the slope as $-E_d/2k_B$, whereas the other workers have taken $-E_d/k_B$.

D. Deep and shallow donors

Figure 5 shows the relative positions of the Γ, L, and X minima as a function of x. Also plotted are the measured values of the Si-donor activation energies of both deep

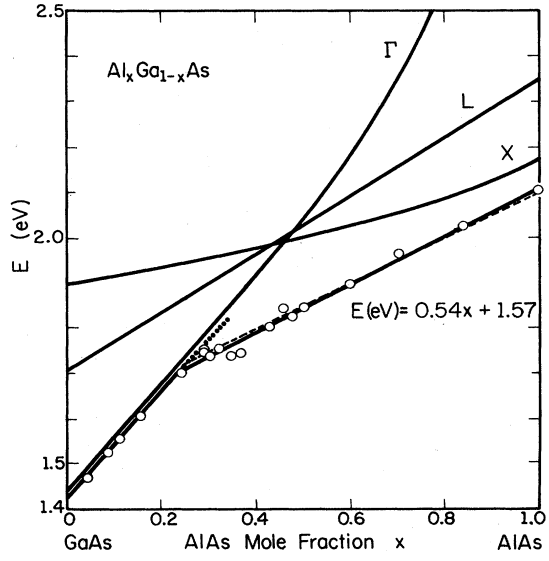

FIG. 5. Variation of Γ-, L-, and X-band energy minima in $Al_xGa_{1-x}As$ as a function of AlAs content x. The solid line through the experimental points represents the position of the Si dominant donor level in the band gap. The dotted line represents the position of the shallow level. The dashed line shows the calculated donor energy level which accounts only for the dominant level.

and shallow levels with respect to the conduction-band minima. The solid line best-fits the experimental points of the deep donor level. The dotted line indicates the position of the shallow level. The dashed line corresponds to the donor position obtained theoretically from a multivalley effective-mass model, as will be described in detail later. For $x \leq 0.20$ the donor level follows the Γ minimum. For $x > 0.20$ the dominant donor energy level with respect to the edge of the valence band increases linearly and can be described by

$$E \cong 0.54x + 1.57 \text{ eV} . \quad (5)$$

At $x \sim 0.2$ the dominant donor level begins to follow the L minima, which indicates that for $x > 0.2$ the donor level associated with the L minima dominates the conduction process, even when the Γ valley is still the conduction-band minimum. With further increasing x, due to the influence of X minima, the donor level no longer follows the L minima. Each conduction band can be considered to be associated with a separate donor level which is shallow for the Γ minimum and deep for the L and X minima. Therefore, for $0.2 \leq x \leq 0.45$, there are effectively two donor levels: a shallow one with the Γ minimum and a deep one with L and X minima. The initial freeze out of electrons in this composition range is to the deep level. When the deep donors are saturated, the freeze out is to the shallow donors. For this reason, samples 1—3 and 5 in the range $0.24 \leq x \leq 0.29$, which are relatively highly doped, having electron concentrations comparable to the conduction-band effective density of states, show an exponential freeze out of carriers through the L minima to the deep donor level. For $T < 150$ K, however, they show metallic behavior since at this point, deep Si donors are saturated and the shallow level is merged with the Γ conduction band.

The shallow level becomes visible below 125 K when the doping level is reduced, as can be seen in Fig. 2 (samples 4 and 6—8). In addition, as in the deep level, the depth of the shallow level below the conduction-band minimum increases with increasing x. This is because the electron effective mass in the Γ minimum increases with x. It should be noted that at low temperatures the conduction may be partly due to phonon-activated hopping between deep donor sites which are unoccupied, but with low mobilities.[24] For alloy compositions $x \geq 0.35$, the conductivity of the layers became unmeasurable at low temperatures for the doping levels studied. This is thought to be due to (i) deepening of the deep and shallow donor levels, (ii) reduced probability of electrons being in the high-mobility Γ minimum, and (iii) deterioration of the Ohmic contacts. It is felt that the shallow level is important only in the range $0.24 \leq x < 0.35$. The ratio of the shallow-level impurity concentration and deep-level concentration decreases with increasing total doping concentration. The growth conditions can undoubtedly have an influence on the respective concentrations of shallow and deep donor levels, which can account for the differences in results reported from different laboratories.

E. Effect of Si-cell temperature

Samples 1 and 2 were grown under similar conditions, with the exception that the Si-effusion-cell temperatures were 1015 and 1100 °C, respectively. The latter sample appears to be highly compensated as it has a relatively higher slope compared to the former sample [Fig. 1(a)]. Owing to broadening of the donor level at high doping densities, sample 2 was expected to have a lower slope than that of sample 1. Compensation in sample 2 is also confirmed by the variation of electron mobility with temperature, and its slope was taken as $-E_d/k_B$, whereas for sample 1 the slope was taken as $-E_d/2k_B$. This suggests that higher Si-cell temperature sometimes leads to higher compensation. Perhaps it is more likely that with increasing Si flux the probability of Si atoms adhering to the As sites increases, resulting in an increased acceptor density. It should be noted that the compensation ratio can be a strong function of the group-V to III- atomic ratio used during growth.

F. Effect of substrate temperature

Comparison of electron densities, mobilities, and persistent photoconductivity in samples 9 and 10, which are nearly of the same composition and were grown at substrate temperatures of 610 and 700 °C, respectively, show less incorporation of Si atoms at high temperatures. The same Si flux was used for both the samples. A similar effect was observed earlier[11] and is attributed to the reduction in the Si sticking coefficient at high substrate temperature.

G. Persistent photoconductivity

In the entire alloy range, with the exception of AlAs, where the effect is negligible, the apparent electron concentration as well as the mobility were found to increase at low temperatures when the samples were exposed to room light. The increase in conductivity persisted even when the light was turned off. This is the well-known persistent-photoconductivity effect,[2,4,19] and is observed in most III-V—compound semiconductors. The samples which were nonconductive in the dark at low temperatures became conductive upon exposure to room light. For a given composition x, persistent carrier density is proportional to the Si atomic density. This indicates that the PPC is, to one extent, related to the Si atoms and not to any background impurity in the crystal. A similar observation was made by Lang *et al.*[4] The increase in carrier density after illumination, Δn, at 77 K, normalized to the Si atomic density, N_{Si}, is plotted in Fig. 6 as a function of x. The solid line in this figure connects the open circles which correspond to $N_{\text{Si}} \leq 3x10^{17}$ cm^{-3}. The solid circles correspond to high values of N_{Si} ($> 10^{18}$ cm^{-3}).

Figure 6 shows that the PPC effect dominates in the range $0.20 \leq x \leq 0.40$, being maximum at $x \sim 0.32$. The solid circles indicate that, for a given x, the ratio $\Delta n/N_{\text{Si}}$ increases with increasing N_{Si}. This means that the fraction of Si atoms responsible for PPC increases with increasing N_{Si}. For $x \geq 0.43$ the PPC carrier density is less than 5% of the Si atomic density. For $0.24 \leq x \leq 0.35$ the persistent electron concentrations at 77 K are higher than the room-temperature electron concentrations. The persistent electron mobilities at 77 K are also higher or com-

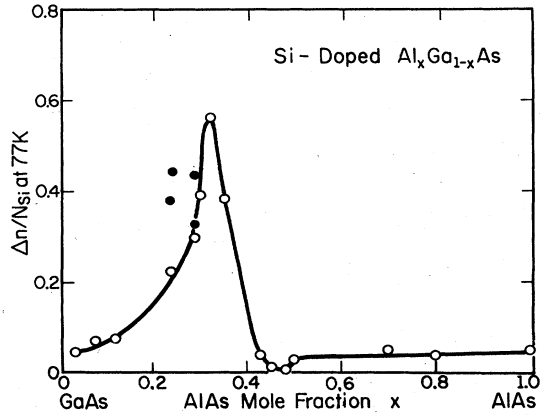

FIG. 6. Persistent change in electron density, after exposure to the ambient light at 77 K normalized to the estimated Si atomic density, is plotted against AlAs mole fraction, x.

parable (Table I) to the room-temperature mobilities and show a considerable increase in some cases over dark values at 77 K.

H. Mobility

The variation of electron mobilities with alloy composition and doping densities at a given x can be seen in Table I. The mobilities are drastically reduced near the direct-indirect crossover composition ($x \sim 0.45$) and remain low for indirect compositions due to the large electron effective mass. For a given alloy composition the mobility decreases with increasing doping densities, as expected. In earlier studies[7] this trend was reversed, due perhaps to the reduction of other defects with increased doping concentration.

IV. THEORY AND DISCUSSION

A. Effect of multivalley conduction on Hall-effect measurements

Owing to the distribution of electrons among all three conduction-band minima Γ, L, and X, which have different mobilities and effective masses, the actual electron concentrations, mobilities, and activation energies may be different from the apparent values plotted in Figs. 1–3. The difference in electron concentration can be estimated as follows.

In a nondegenerate material, the electron concentration in the i valley (Γ, L, or X) is given by

$$n_i = 2\left[\frac{2\pi m_i^* k_B T}{h^2}\right]^{3/2} \exp\left[-\frac{E_i - E_F}{k_B T}\right], \tag{6}$$

where $E_i - E_F$ is the energy difference between the i-valley minimum and the Fermi level. The total carrier density will be

$$n = n_\Gamma + n_L + n_X , \tag{7}$$

and the fraction of electrons in the i valley is

$$f_i = n_i / n ,$$

e.g.,

$$f_\Gamma = \left[1 + \left[\frac{m_L^*}{m_\Gamma^*}\right]^{3/2} \exp\left[-\frac{\Delta E^{L-\Gamma}}{k_B T}\right] + \left[\frac{m_X^*}{m_\Gamma^*}\right]^{3/2} \exp\left[-\frac{\Delta E^{X-\Gamma}}{k_B T}\right]\right]^{-1} . \tag{8}$$

Similar expressions for f_L and f_X describing the fraction of electrons in L and X valleys can be written easily. Using the values of m_i^*, and E_i given in Ref. 22, f_i was calculated and is plotted in Fig. 7 as a function of x for 300, 150, and 50 K. Minor variations of effective masses and band-gap differences with temperature were ignored. Figure 7 indicates that at room temperature more than 95% of the electrons are either in the Γ valley if $x \leq 0.2$, or in the X valley if $x \geq 0.6$. For alloy compositions $0.2 \leq x \leq 0.6$ the electrons are shared in all three valleys. As the temperature is lowered, f_L decreases, whereas f_Γ or f_X increases, and at 50 K most of the electrons are either in the Γ or X valley, depending on the composition. Thus, during cooling, the electrons from the L valley are expected to freeze out first. As the electrons from the L minima are captured by the deep donor impurities, more electrons are scattered into the L minima from the Γ and X minima to maintain the statistical equilibrium.

From Fig. 7 it is clear that appreciable differences between the true electron concentrations (n_T) and the apparent (Hall) concentrations (n_H) are expected only in the range $0.2 \leq x \leq 0.6$. The ratio n_T/n_H is given by[6]

$$\frac{n_T}{n_H} = \frac{f_\Gamma \mu_{H\Gamma}^2 + f_L \mu_{HL}^2 + f_X \mu_{HX}^2}{(f_\Gamma \mu_{H\Gamma} + f_L \mu_{HL} + f_X \mu_{HX})^2} , \tag{9}$$

where μ_{Hi} is the Hall mobility in the i valley. Obviously, for $0.2 \geq x \geq 0.6$, $n_T \cong n_H$. Taking typical values of mobilities for different valleys as $\mu_{H\Gamma} = 2500\ \mathrm{cm^2 V^{-1} s^{-1}}$, $\mu_{HL} = 400\ \mathrm{cm^2 V^{-1} s^{-1}}$,[6] and $\mu_{HX} = 150\ \mathrm{cm^2 V^{-1} s^{-1}}$,

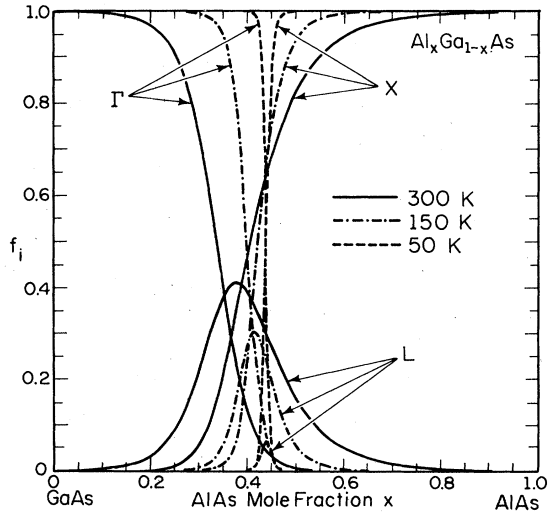

FIG. 7. Fractional distribution of electrons in Γ, L, and X valleys as a function of alloy composition x at 300, 150, and 50 K.

n_T/n_H has been calculated at room temperature and plotted in Fig. 8 as a function of x. $\mu_{H\Gamma}$ and μ_{HX} were estimated using the measured values of μ for $x<0.2$ (GaAs-rich side) and $x>0.6$ (AlAs-rich side), respectively. All the terms in Eq. (9) are functions of temperature and it is not straightforward to evaluate the variation of n_T/n_H with temperature. Since at low temperatures (<100 K) most of the electrons are either in the Γ or X valley for $x<0.45$ and $x>0.45$, respectively, the ratio n_T/n_H should approach unity as the temperature decreases. Thus, at low temperatures the difference between n_T and n_H which is significant only for the range $0.25\leq x\leq 0.6$ should be smaller than that shown in Fig. 8. Here, it is worth pointing out that the values of N_d consistent with the Si atomic concentrations are obtained only if the true electron concentrations, n_T (and not the n_H), are used in Eq. (1) at room temperature.

The activation energies described earlier were measured between 300 and 150 K. Assuming that the electron mobilities at 300 and 150 K are the same, the ratio n_T/n_H was also evaluated at 150 K and plotted in Fig. 8. A comparison of the 300- and 150-K curves in Fig. 8 shows that n_T/n_H does not vary substantially except at $x\sim 0.4$. Actual electron concentration may be different, but an almost constant ratio n_T/n_H or a slight variation in n_T/n_H will have a negligible effect on the slope of the curves in Figs. 1 and 2, and hence the activation energies in Fig. 4 will remain approximately unchanged.

In devices such as modulation-doped field-effect transistors, the actual electron concentration, n_T not n_H, must be used when E_F is above the donor level, and N_d must be used when E_F is below the donor level. In addition, in modeling such devices, in the wide range of temperatures used, a simple activation energy should not be used because activation energies reported here and elsewhere are in most cases good for the temperature range of 150–300 K. The measured activation energies appear to vary somewhat depending on the growth conditions, the compensation, and the doping densities used. In the compensated samples the electrons not only experience a Coulomb force due to positively charged donors, but also another Coulomb force due to negatively charged acceptors, which affects the activation energy. For $x\cong 0.29$, a commonly used alloy for MODFET's, the electron concentration saturates below 150 K, and E_d ($150<T<300$ K) is ≈ 48–66 meV for the doping densities employed here.

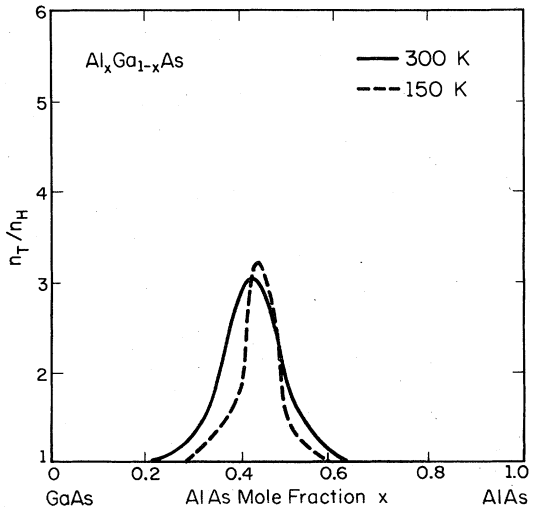

FIG. 8. Effect of multivalley conduction on the measured electron concentration. The ratio of true electron concentration, n_T, and the measured Hall concentration, n_H, is plotted as a function of alloy composition x for $Al_xGa_{1-x}As$ at 300 (solid line) and 150 K (dashed line).

B. Activation energy (multivalley effective-mass model)

The alloy-composition dependence of Si-donor activation energy is quite similar to what has been observed for other donor dopants, such as Se, Te, and Sn in LPE- and organometallic vapor-phase-epitaxy—(OMVPE)-grown $Al_xGa_{1-x}As$. It can then be concluded that, in general, the activation energy of commonly used donors in $Al_xGa_{1-x}As$ is relatively independent of the nature of the donor species and the growth technique used.

The variation of E_d with x is largely due to changes in the conduction-band structure. Both the electron effective mass and the dielectric constant change with x, and this change affects the Coulomb binding energy of the electrons to the donor atoms. To a first approximation the binding energy E_d in a simple effective-mass model can be given by

$$E_d=\left[\frac{m^*}{m_0}\right]\frac{E_H}{\epsilon_s^2}\ , \tag{10}$$

where m^* is the spherical effective mass of the conduction-band electron and ϵ_s is the static dielectric constant of the semiconductor. E_H (13.6 eV) is the ionization energy for the ground-state hydrogen atom. In a semiconductor with a multivalley conduction band, however, Eq. (10) is not valid and will generally greatly underestimate the true donor binding energy. Thus, for $Al_xGa_{1-x}As$, in which at various x the Γ, X, and L minima must all be considered, we need a more careful and complete theoretical treatment in order to properly explain the donor binding energies.

We begin with the single-band effective-mass approximation (EMA). The EMA Hamiltonian is given by

$$H=H_0+V\ , \tag{11}$$

where H_0 is the Hamiltonian of the crystal without any impurity and V is the potential due to the donor atoms. The EMA envelope function in $\vec{k}$ space is written as a sum of terms located at the Γ-, X-, and L-symmetry points,

$$F(\vec{k})=F_\Gamma(\vec{k})+\sum_{i=1}^{3}F_X(\vec{k}-\vec{k}_i^{\,X})+\sum_{j=1}^{4}F_L(\vec{k}-\vec{k}_j^{\,L})\ , \tag{12}$$

where $\{\vec{k}_i^{\,X},\ i=1,2,3\}$ denote the three X points and $\{\vec{k}_j^{\,L},\ j=1,2,3,4\}$ denote the four L points. Because the envelope function is located at various $\vec{k}$, we must include the intervalley scattering contribution.

The envelope function may be Fourier-transformed and written in terms of $\vec{r}$ rather than $\vec{k}$. Thus,

$$F(\vec{r})=F_\Gamma(\vec{r})+\sum_{i=1}^{3}F_X(\vec{r})\exp(i\vec{k}_i^X\cdot\vec{r})+\sum_{j=1}^{4}F_L(\vec{r})\exp(i\vec{k}_j^L\cdot\vec{r}) , \quad (13)$$

where $F_\Gamma(\vec{r})$, $F_X(\vec{r})$, and $F_L(\vec{r})$ are chosen to be linear combinations of ten exponential functions; for example,

$$F_\Gamma(\vec{r})=\sum_{j=1}^{10}C(\Gamma,j)\exp(-\alpha_j r) , \quad (14)$$

where $C(\Gamma,j)$ is a variational parameter and the α_j's are chosen to cover a large realistic range. The terms of F_X and F_L can be similarly defined. The kinetic-energy term of the Hamiltonian for a given valley is now written as

$$-\frac{\hbar^2}{2m^*}\nabla_r^2+E_0 , \quad (15)$$

where m^* is the spherical effective mass appropriate for the valley under consideration and E_0 is the energy minimum for that valley. We determined the spherical effective masses for GaAs and AlAs at X and L by calculating the transverse and longitudinal masses m_t^* and m_l^* using a local pseudopotential theory and the parameters of Refs. 25 and 26. The value of m^* is determined by requiring that the binding energy of a spherical hydrogenic system with mass m^* agree with the result of Kohn and Luttinger[27] for the correct anisotropic masses. The value of m^* so obtained is, in general, different from the density-of-states effective mass used elsewhere in this study. The resulting values are listed in Table II. We find, however, that a better agreement with the data can be obtained if we modify $m^*(L)$ for GaAs from $0.22m_0$ to $0.27m_0$. This modification is not unreasonable, considering the uncertainty in the pseudopotential model.

The impurity potential is given by

$$V(\vec{r})=\frac{-e^2}{\epsilon(r)r}(1-e^{-r/r_c}) , \quad (16)$$

where $\epsilon(r)$ is the dielectric function written in the following empirical form:[28]

$$\frac{1}{\epsilon(r)}=\sum_{\nu=1}^{4}S_\nu\exp(-\sigma_\nu r) . \quad (17)$$

The numbers S_ν and σ_ν are the constants chosen to correctly describe the function $\epsilon(r)$. The term e^{-r/r_c} produces a cutoff of the Coulomb potential for small r to mimic the central-cell short-range potential, and serves to stabilize the variational calculation.[29] The core radius r_c is empirically fitted to the correct energy for one alloy composition.

The matrix elements of the intervalley potential-energy term must be modified due to the effect of umklapp scattering. Altarelli *et al.*[30] have shown that the effect of the umklapp scattering is equivalent to multiplying the intervalley potential-energy term between valleys i and j by a renormalization factor $R(i,j)$ defined as

$$R(i,j)=\sum_{\vec{G}}C(\vec{k}_i,\vec{k}_j,\vec{G})\frac{|\vec{k}_i-\vec{k}_j|^2\epsilon(\vec{k}_i-\vec{k}_j)}{|\vec{k}_i-\vec{k}_j-\vec{G}|^2\epsilon(\vec{k}_i-\vec{k}_j-\vec{G})} , \quad (18)$$

where $\epsilon(\vec{q})$ is the $\vec{q}$-dependent dielectric function. The $C(\vec{k}_i,\vec{k}_j,\vec{G})$'s are the plane-wave–expansion coefficients for the product $U^*_{\vec{k}_i}(\vec{r})U_{\vec{k}_j}(\vec{r})$, where $U^*_{\vec{k}_i}(\vec{r})$ and $U_{\vec{k}_j}(\vec{r})$ are the periodic parts of the electronic Bloch states at $\vec{k}_i$ and $\vec{k}_j$, respectively. We calculate the renormalization coefficient $R(i,j)$ using the pseudopotential method with 89 plane waves, $\epsilon(\vec{q})$ for AlAs as given in Ref. 31 for GaP but normalized to $\epsilon_s=10.4$, and $\epsilon(\vec{q})$ for GaAs as given in Ref. 31 with $\epsilon_s=12.6$. The results are summarized in Table III. The matrix element of $U(\vec{r})$ evaluated between F_i and F_j (where i and j are Γ, X, and L) is then

$$\langle F_i|U(\vec{r})|F_j\rangle=-R(i,j)\left\langle F_i\left|\sum_{\nu=1}^{4}S_\nu\exp(-\sigma_\nu r)\frac{e^2}{r}(1-e^{-r/r_c})\right|F_j\right\rangle . \quad (19)$$

The expectation value of the Hamiltonian is thus found within the multivalley EMA as a function of the variational parameters and minimized. In this way the donor binding energy in $Al_xGa_{1-x}As$ is calculated as a function of x. The energies of the bottom of the conduction-band minima for GaAs and AlAs are also given in Table II. For alloys with $x<0.45$ we used a linear interpolation of all energies and masses between GaAs and AlAs, and for alloys with $x>0.45$ the band gap E_g was taken as

$$E_g=1.424+1.247x+1.147(x-0.45)^2 \text{ eV} . \quad (20)$$

The donor binding energy is the difference between the calculated donor energy and the bottom of the lowest

TABLE II. Energy gaps and effective masses for GaAs and AlAs.

	GaAs	AlAs
E_g^Γ	1.424 eV	3.018 eV
E_g^L	1.708 eV	2.35 eV
E_g^X	1.900 eV	2.168 eV
$m^*(\Gamma)$	$0.067m_0$	$0.15m_0$
$m^*(L)$	$0.22m_0$ ($0.27m_0$)[a]	$0.27m_0$[a]
$m^*(X)$	$0.60m_0$	$0.38m_0$

[a]Modified value which best fits the experimental data.

TABLE III. Renormalization factors.

	$R(i,j)$	
$\vec{k}_i,\vec{k}_j$	AlAs	GaAs
$\Gamma-\Gamma$	1.0	1.0
$\Gamma-L$	1.13	1.28
$X-X$	0.75	0.78
$L-L$	1.2	1.41
$X-L(1)$	0.32	0.08
$X-L(2)$	0.46	0.41

conduction-band valley. The value of r_c was determined to be 1.01 Å by fitting the binding energy at the direct-indirect crossover point, i.e., $x=0.45$ to 160 meV. The values of binding energy obtained this way are plotted in Figs. 4 and 5 and are in good agreement with the measured values. The large binding energies for $x\sim0.45$—0.48 are due largely to the intervalley scattering in the X and L valleys. This lowers the donor energy level in the band gap (i.e., enhances the binding energy) which tends to further localize the electron wave function in real space and delocalize it in momentum space. The localization in real space lowers the energy because the Coulomb potential is not screened so strongly; the delocalization in $\vec{k}$ space further lowers the energy because the intervalley scattering is enhanced. Such behavior cannot be explained without correctly including the intervalley scattering and the $\vec{q}$ dependence of the dielectric function.

C. Persistent photoconductivity

As shown in Table I and plotted in Fig. 6 the PPC effect is observed in the entire AlAs mole-fraction range, but the effect is greatest in the range $0.20\leq x\leq0.4$ and smallest in the direct-indirect crossover region. If the Si-doping density is reduced, persistent-photoelectron density is also reduced and *vice versa*. Lang *et al.*[4,32] observed a dependence of the PPC on the type of donor species, and their Si- and Sn-doped samples exhibited behavior somewhat different from that of Se- and Te-doped samples. By virtue of a decrease in mobility, these authors and Nelson[2] attributed the PPC effect to the presence of some donor-vacancy- (*DX*-) type trap centers, which themselves behaved as donors. The depth of the Si-related *DX* centers was noted to be deeper than of the Te- and Se-related centers.

The *DX*-type traps can easily explain the increase in carrier density,[2,4,32] but they cannot explain the corresponding increase in mobility after photoexcitation. Donor-type traps should lead to a decrease in mobility after emission of electrons due to increased ionized-impurity scattering from the charged donor impurity atoms which are otherwise neutral when occupied. Te and Se, which come from column VI of the Periodic Table, primarily behave as donors in III-V compounds, whereas Sn and Si are amphoteric impurities and can behave both as donors and acceptors, depending upon the growth conditions used. As the study of Lang *et al.*[4] was largely based on Te doping, it is possible that the traps associated with Te may be of donor type. Traps associated with Si, however, appear most likely to be of double-acceptor type. If so, their concentration is maximum at $x\sim0.32$ and increases at a faster rate with increasing doping density.

Persistent photoconductivity and an increase in electron mobility upon photoexcitation at low temperatures was also observed in $GaAs_{1-x}P_x$ (Ref. 20) and $Cd_{1-x}Zn_xTe$ (Ref. 33). The presence of double acceptors changing the charge state from -2 to -1 upon emission of the electrons to the conduction band was suggested as the mechanism responsible. This reduces the ionized-impurity scattering, resulting in an increase in mobility. Furthermore, since the acceptor centers are still negatively charged, they act as a Coulomb barrier to the electrons in the conduction band, resulting in the observed persistent photoconductivity. The same mechanism was proposed by Künzel *et al.*[10] and Saxena[19] for AlGaAs. Künzel *et al.*,[18] in their most recent paper, have, however, suggested *DX*-type centers to be responsible for the PPC.

The enhancement of mobility can be explained only partially by an increased screening of impurities by photogenerated carriers. Moreover, if the scattering in the dark at low temperatures is due to positively charged centers, then as the electron concentration increases due to photoexcitation from acceptor-type traps, the Fermi level rises and these positively charged centers become filled with electrons, further reducing the number of scattering centers and enhancing the mobility.

Saxena[19] also suggested that in direct-gap alloys, upon photoexcitation at low temperatures, the electrons are emitted from the deep impurity level (attached to the L band) to the L minima, and from there they are scattered into the Γ minimum, perhaps to maintain the statistical equilibrium. As shown in Fig. 9, due to the indirect nature of the transitions involved between the Γ minimum and the deep states, and the small value of f_L at low temperature (Fig. 7), the electrons in the Γ minimum are prohibited from either falling back to the deep states or being scattered back to the L minima, respectively, thus showing persistent photoconductivity. Upon increasing the temperature, the electrons are transferred from the Γ minimum to the L minima, and from there they can fall back into the deep states, reducing the effect of the persistent photoconductivity.

If the above model of Saxena's is true, we propose an explanation for the other related observed effects, viz., the increase in mobility, dependence of PPC on the doping density, and alloy composition. At low temperatures in the dark the conduction in $Al_xGa_{1-x}As$ partly occurs by phonon-activated hopping between donor sites which are unoccupied due to the presence of compensating impurities. The mobility associated with the impurity conduction is relatively small, and thus the measured effective mobilities are also small. Upon photoexcitation the elec-

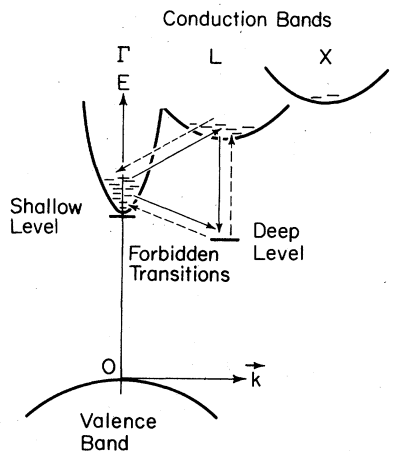

FIG. 9. Approximate band structure of direct-band-gap $Al_xGa_{1-x}As$. The solid and dashed arrows represent the various possibilities for electron capture and emission by the deep level, respectively. (After Saxena, Ref. 19.)

trons are transferred to the Γ valley where the electrons' mobility is much higher, and thus an increase in mobility is observed upon photoexcitation. This is apparent from Table I where the Hall mobilities in all direct-gap alloys after light illumination at 77 K are of the same order except for some differences due to different doping levels representing the conduction in the Γ valley. As the L and X minima play no role for $x<0.2$, and the Γ minimum plays no role for $x>0.45$, the observed PPC effect is negligible for these compositions and is similar to what is commonly observed in all III-V compounds. As x is increased from 0.2, the effect of the L and X minima increases, whereas the donor level associated with the Γ minimum to which the electrons can fall back remains shallow, the PPC effect increases with x. For $x>0.32$, (i) the occupancy factor of the L and X minima increases so that a relatively lower number of electrons is scattered into the Γ minimum, and (ii) the shallow donor level attached to the Γ minimum deepens so that more electrons can be captured by the shallow level although the electrons were originally emitted from the deep level. This explains why the PPC decreases for $x>0.32$. As stated in an earlier section, the ratio of the deep-level concentration to the shallow-level concentration increases with increasing doping density. Because of this, with increasing doping density a relatively large number of carriers is excited from the deep level to the Γ minimum through the L or X minima, and so the PPC increases, as observed (shown by the solid circles in Fig. 6).

The above model does not explain the necessity of an optical energy of ~ 1.1 eV to observe the PPC effect.[2,4] It is possible that Γ and L valleys overlap at some energy level and the transition of electrons from the L to the Γ valley occurs at that energy level, thus requiring a minimum optical energy for the PPC to be observed. If this is so, the threshold optical energy should be composition dependent. In addition, upon application of a suitable hydrostatic pressure which will move the Γ minimum to higher energies, no persistent photoconductivity should be observed. This is left for future work.

We believe that the formation of a two-dimensional electron gas (2DEG) and the transfer of electrons to the 2DEG after photoexcitation at the $Al_xGa_{1-x}As/GaAs$ interface alone, as proposed by Collins *et al.*,[14] cannot explain the observed PPC results for the following reasons:

(a) To ensure that the increase in mobility was not due to any fraction of charge transfer to the $GaAs/Al_xGa_{1-x}As$ interface, in some cases we employed compositional grading in the buffer layers to prevent any remote possibility of 2DEG formation. An increase in mobility in these samples also confirmed that the observed PPC effects are not due to any two-dimensional electron gas.

(b) The mobilities listed in Table I suggest that the transport properties of carriers have not changed significantly upon photoexcitation, except for some increase in mobilities. The mobilities still represent the carriers in the $Al_xGa_{1-x}As$.

(c) However, if there was some contribution from the 2DEG, calculations show that due to relatively large mobilities in the 2DEG, in most cases the actual values of carrier densities and mobilities in the $Al_xGa_{1-x}As$ should be higher and lower, respectively, than the measured values shown in Table I at all temperatures both in the dark and light. The actual persistent electron densities in $Al_xGa_{1-x}As$ will then be higher than the apparent values of Table I.

(d) Most importantly, cyclotron-resonance measurements on a highly-light-sensitive sample did not show any free carrier with mobility greater than 2000 $cm\,V^{-1}s^{-1}$. This confirmed the absence of any 2DEG.

More work needs to be done to ascertain the exact cause of the persistent photoconductivity.

V. CONCLUSIONS

The free-electron concentration in Si-doped $Al_xGa_{1-x}As$ ($x=0$ to 1) shows an exponential dependence on temperature. There appears to be both a shallow and a deep Si donor, the ionization energy of which varies with the alloy composition x and changes markedly for alloy compositions in the neighborhood of the direct-indirect crossover. The depth of both deep and shallow donor levels below the conduction-band minimum decreases with increasing doping levels. A multivalley effective-mass model has been successfully used to explain the observed variation of ionization energy. The dominant deep donor levels are coupled to the higher-energy indirect L and X minima even for alloy compositions in which the Γ minimum is the lowest in energy. The Si-donor level behaves in a manner similar to that of Te, Se, and Sn, and is independent of the growth technique employed. A fewer number of Si atoms is incorporated into the layer at high substrate-growth temperatures. The electron mobility decreases near the direct-indirect crossover and remains low for higher-x composition due largely to the increased electron effective mass.

The persistent-photoconductivity effect is observed over the entire composition range, particularly between $x=0.2$ and 0.4, with an increase in mobility at temperatures <100 K. Acceptor-like deep traps may be responsible for the observed PPC. Band-structure effects, in which the electrons are captured in the L or X valley from the deep donor levels and are rapidly thermalized into the Γ minimum from where they are prohibited from being recaptured, have also been used to explain the observed properties of the PPC.

ACKNOWLEDGMENTS

We wish to thank P. Pearah, C. Goetschell, and W. Kopp for help in Hall-effect and PL measurements, Professor D. Tsui for carrying out cyclotron-resonance measurements, and C. Begg for carrying out the wavelength-dispersive x-ray analysis. We are grateful to Dr. F. Ponse, Dr. F. Stern, Dr. D. C. Reynolds, Dr. K. K. Bajaj, Dr. C. W. Litton, and Dr. J. Singh for fruitful discussions. This

work was funded by the U.S. Air Force Office of Scientific Research and the U.S. Joint Services Electronics Program, and the U.S. Office of Naval Research under Contract No. N000014-81-K-0430. The authors would also like to express their gratitude to Dr. K. J. Malloy for supplying us with a copy of his Ph.D. thesis, which also deals with donor incorporation in $Al_xGa_{1-x}As$ and for fruitful discussions.

[1]A. J. SpringThorpe, F. D. King, and A. Becke, J. Electron. Mater. **4**, 101 (1975).
[2]R. J. Nelson, Appl. Phys. Lett. **31**, 351 (1977).
[3]M. Ayabe, Y. Mori, and M. Watanabe, Jpn. J. Appl. Phys. **20**, L55 (1981).
[4]D. V. Lang, R. A. Logan, and M. Jaros, Phys. Rev. B **19**, 1015 (1979).
[5]J. J. Yang, L. A. Mandy, and W. I. Simpson, Appl. Phys. Lett. **40**, 244 (1982).
[6]N. Lifshitz, A. Jayaraman, and R. A. Logan, Phys. Rev. B **21**, 670 (1980).
[7]H. Morkoç, A. Y. Cho, and C. Radice, J. Appl. Phys. **51**, 4882 (1980).
[8]Y. G. Chai, R. Chow, and C. E. C. Wood, Appl. Phys. Lett. **39**, 800 (1981).
[9]T. Ishikawa, J. Saito, S. Sasa, and S. Hiyamizu, Jpn. J. Appl. Phys. **21**, L675 (1982).
[10]H. Künzel, H. Jung, E. Schubert, and K. Ploog, J. Phys. (Paris) Colloq. **43**, C5-175 (1982).
[11]T. J. Drummond, W. G. Lyons, R. Fischer, R. E. Thorne, and H. Morkoç, J. Vac. Sci. Technol. **21**, 957 (1982).
[12]R. Fischer, C. G. Hopkins, C. A. Evans, Jr., T. J. Drummond, W. G. Lyons, J. Klem, C. Colvard, and H. Morkoç, in *GaAs and Related Compounds,* edited by G. E. Stillman (IOP, Bristol, 1982), p. 157.
[13]R. E. Thorne, T. J. Drummond, W. G. Lyons, R. Fischer, and H. Morkoç, Appl. Phys. Lett. **41**, 189 (1982).
[14]D. M. Collins, D. E. Mars, B. Fischer, and C. Kocot, J. Appl. Phys. **54**, 857 (1983).
[15]M. Heiblum, W. I. Wang, L. E. Osterling, and V. Deline, J. Appl. Phys. **54**, 6751 (1983).
[16]K. Ploog, in *Crystals,* edited by H. C. Freyhardt (Springer, Berlin, 1980), Vol. 3, p. 73.
[17]A. K. Saxena, Phys. Status Solidi B **105**, 777 (1981).
[18]H. Künzel, K. Ploog, K. Wünstel, and B. L. Zhou, J. Electron. Mater. **13**, 281 (1984).
[19]A. K. Saxena, Solid State Electron. **25**, 127 (1982).
[20]M. G. Craford, G. E. Stillman, J. A. Rossi, and N. Holonyak, Jr., Phys. Rev. **168**, 867 (1968).
[21]A. Chandra, C. E. C. Wood, D. W. Woodard, and L. F. Eastman, Solid State Electron. **22**, 645 (1979).
[22]H. C. Casey, Jr. and M. B. Panish, *Heterostructure Lasers, Part A: Fundamental Principles* (Academic, New York, 1978).
[23]A. K. Saxena and B. B. Singh, Phys. Rev. B **28**, 1132 (1983).
[24]N. F. Mott and W. D. Twoso, Adv. Phys. **10**, 107 (1961).
[25]M. L. Cohen and T. K. Bergstresser, Phys. Rev. **141**, 789 (1966).
[26]E. Hess, I. Topol, K. R. Schulze, H. Neumann, and K. Unger, Phys. Status Solidi B **55**, 187 (1973).
[27]W. Kohn and J. M. Luttinger, Phys. Rev. **98**, 915 (1955).
[28]S. T. Pantelides and C. T. Sah, Phys. Rev. B **10**, 621 (1974).
[29]Without the cut off term, the variational calculation will be unstable because of the neglect of the intervalley kinetic-energy term. However, the effect of the intervalley kinetic-energy term is small compared to the intervalley potential-energy term once the calculation is stabilized by introducing a cutoff in the Coulomb potential.
[30]M. Altarelli, W. Y. Hsu, and R. A. Sabatini, J. Phys. C **10**, L605 (1979).
[31]P. K. W. Vinsome and D. Richardson, J. Phys. C **4**, 2650 (1971).
[32]D. V. Lang and R. A. Logan, Phys. Rev. Lett. **39**, 635 (1977).
[33]B. C. Burkey, R. P. Khosla, J. R. Fischer, and D. L. Losee, J. Appl. Phys. **47**, 1095 (1976).